Unique size-dependent nanocatalysis revealed at the single atomically precise gold cluster level

Yuwei Zhang[a,b,1], Ping Song[a,b,1], Tiankai Chen[c], Xiaodong Liu[a,b,d], Tao Chen[a,b,d], Zhemin Wu[e,f], Yong Wang[e,f], Jianping Xie[c,2], and Weilin Xu[a,b,2]

[a]State Key Laboratory of Electroanalytical Chemistry, Changchun Institute of Applied Chemistry, Chinese Academy of Sciences, Changchun 130022, China; [b]Jilin Province Key Laboratory of Low Carbon Chemical Power, Changchun Institute of Applied Chemistry, Chinese Academy of Sciences, Changchun 130022, China; [c]Department of Chemical and Biomolecular Engineering, National University of Singapore, Singapore 117585; [d]University of Chinese Academy of Sciences, Beijing 100049, China; [e]Center of Electron Microscopy, School of Materials Science and Engineering, Zhejiang University, Hangzhou 310027, China; and [f]State Key Laboratory of Silicon Materials, School of Materials Science and Engineering, Zhejiang University, Hangzhou 310027, China

Atomically precise metal clusters have attracted increasing interest owing to their unique size-dependent properties; however, little has been known about the effect of size on the catalytic properties of metal clusters at the single-cluster level. Here, by real-time monitoring with single-molecule fluorescence microscopy the size-dependent catalytic process of individual Au clusters at single-turnover resolution, we study the size-dependent catalytic behaviors of gold (Au) clusters at the single-cluster level, and then observe the strong size effect on the catalytic properties of individual Au clusters, in both catalytic product formation and dissociation processes. Surprisingly, indicated by both experiments and density functional theory (DFT) calculations, due to such a unique size effect, besides observing the different product dissociation behaviors on different-sized Au clusters, we also observe that small Au clusters [i.e., $Au_{15}(MPA)_{13}$; here, MPA denotes 3-mercaptopropionic acid] catalyze the product formation through a competitive Langmuir–Hinshelwood mechanism, while those relatively larger Au clusters [e.g., $Au_{18}(MPA)_{14}$ and $Au_{25}(MPA)_{18}$] or nanoparticles catalyze the same process through a noncompetitive Langmuir–Hinshelwood mechanism. Such a size effect on the nanocatalysis could be attributed intrinsically to the size-dependent electronic structure of Au clusters. Further analysis of dynamic activity fluctuation of Au clusters reveals more different catalytic properties between Au clusters and traditional Au nanoparticles due to their different size-dependent structures.

single-molecule nanocatalysis | gold clusters | single-molecule fluorescence microscopy | size dependence | quantum effect

Due to the limited resources of gold (Au) on earth, we need to minimize the usage of Au by extracting its highest possible catalytic activity on the Au atom basis (1–4). To achieve this, significant work has been done to examine size-dependent catalysis of Au nanoparticles (5–7). Compared with traditional ensemble methods, the single-molecule, single-particle method can give deeper insight by removing ensemble averaging, thus uncovering heterogeneous and dynamic behaviors of individual nanoparticles that are often hidden in ensemble-averaged measurements (8–13). For this reason, in recent years, the method of single-molecule nanocatalysis based on single-molecule fluorescence microscopy has been used extensively to investigate the size-dependent catalytic kinetics and dynamic behaviors of single metal nanoparticles (e.g., platinum, palladium, and gold) at the single-molecule, single-particle level (6, 14–17). Atomically precise Au clusters with well-defined size and structure could perfectly match with the single-molecule fluorescence microscopy technique to uncover several challenging fundamental issues in Au nanocatalysts. In particular, ultrasmall Au clusters often feature unique size effects (18) due to their size-dependent electronic structures (19, 20) and work functions (21), etc. The catalytic properties of Au clusters are highly dependent on (and sensitive to) their sizes due to the size-sensitive electronic structures (such as charge density profile), which are distinctly different from their larger counterparts, traditional Au nanoparticles with a large numbers of

Au atoms. However, little is known about the size effect on catalytic properties of Au clusters at the single-molecule, single-particle level, although the synthesis of such atomically precise Au clusters with different sizes has been well developed in the cluster community (5, 22–24).

To study the size effect on catalytic properties of Au clusters with precise number of atoms (at atomic precision), here we chose three different sized thiolate-stabilized Au clusters—$Au_{15}(MPA)_{13}$, $Au_{18}(MPA)_{14}$, and $Au_{25}(MPA)_{18}$—as model catalysts (MPA denotes 3-mercaptopropionic acid). A gold-catalyzed fluorogenic reaction (i.e., reduction of nonfluorescent resazurin to fluorescent resorufin) was chosen as a probe to study the catalytic kinetics and dynamics of individual Au clusters of different sizes, leveraging on the powerful single-molecule fluorescence microscopy. Strong size-dependent catalytic behaviors of Au clusters were observed in both catalytic product formation and dissociation processes. The size-dependent catalytic activities and mechanisms could be attributed to the size-dependent adsorption behaviors of the substrate and product molecules on Au clusters, which are induced by the size-dependent electronic structures of Au clusters.

Results and Discussion

Catalytic Kinetics of Individual Clusters in Different Sizes. Water-soluble Au clusters protected by MPA with different sizes [e.g., $Au_{15}(MPA)_{13}$, $Au_{18}(MPA)_{14}$, and $Au_{25}(MPA)_{18}$] were synthesized according to a reported protocol (25). UV-Vis absorption and electrospray ionization (ESI) mass spectra (Fig. 1A and *SI*

Significance

Here, by real-time monitoring with single-molecule fluorescence microscopy the size-dependent catalytic process of individual Au clusters at single-turnover resolution, we study the size-dependent catalytic behaviors of gold (Au) clusters at the single-cluster level, and then observe the strong unique size effect on the catalytic properties of individual Au clusters, in both catalytic product formation and dissociation processes. Such a unique size effect on the nanocatalysis could be attributed intrinsically to the size-dependent electronic structure of Au clusters, leading to a more comprehensive understanding of the catalytic mechanism of Au particles.

Appendix, Fig. S1) confirmed the successful synthesis of Au$_{15}$ (MPA)$_{13}$, Au$_{18}$(MPA)$_{14}$, and Au$_{25}$(MPA)$_{18}$ with high purity (hereafter denoted as Au$_{15}$, Au$_{18}$, and Au$_{25}$ clusters, respectively). TEM images (Fig. 1*B*) further support the ultrasmall size of Au clusters used in this study. Similar to the traditional Au nanoparticles (6, 14), the as-prepared Au clusters can effectively catalyze the reduction of nonfluorescent resazurin to fluorescent resorufin by the reductant hydroxylamine (NH$_2$OH), as shown in Fig. 1*C* (14). Control experiments further indicate that only the gold atoms rather than the ligand MPA are the active components for the catalysis. The remarkable stability of ligand MPA on Au clusters or the Au clusters on slide during the catalysis was also confirmed by the X-ray photoelectron spectroscopy (XPS) and size analysis before and after the long-term (6 h) ensemble catalytic process (*SI Appendix*, Fig. S2).

In a typical single-molecule experiment setup (Fig. 2*A* and *SI Appendix*, Scheme S1), the as-prepared Au clusters were first dispersed sparsely (*SI Appendix*, Fig. S3) on a quartz slide surface, followed by an overnight flowthrough of pure water to remove any extra MPA from the cluster surface before flow in the reactant solution. By detecting the fluorescence of individual resorufin molecule formed locally on the surface of individual Au clusters (*SI Appendix*, Fig. S4), we can monitor the catalytic behaviors of individual Au clusters at single-turnover resolution under ambient reaction conditions. Fig. 2*B* shows a typical fluorescence trajectory during the catalytic reaction, reflecting the product formation process (τ_{off}) and dissociation process (τ_{on}) on an individual Au cluster. The digital nature of the stochastic off–on fluorescence bursts and the consistent height of the on level are characteristics of single-molecule fluorescence detection. τ_{off} is the time before each burst, and it is the time for
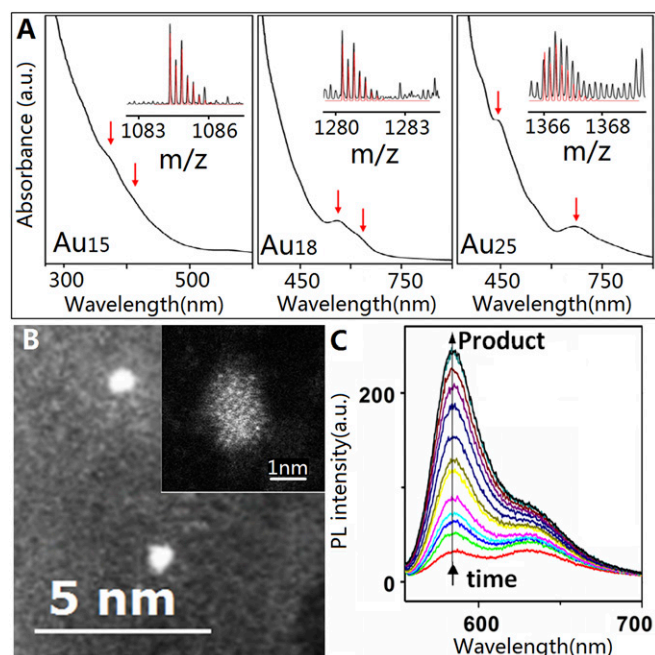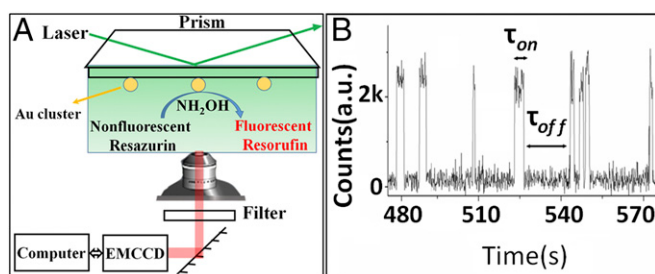

Fig. 2. Single-turnover detection of single Au cluster catalysis. (*A*) Experimental design using total internal reflection fluorescence microscopy for single-molecule, single-particle measurement. (*B*) A typical fluorescence turnover trajectory of a single Au$_{25}$ cluster with 100-ms imaging rate. a.u., arbitrary units.

the formation of each fluorescent product on an individual Au cluster. τ_{on} is the time required for the dissociation of each fluorescent product from the Au cluster surface after its formation. Each off–on cycle corresponds to a single turnover of catalytic process. According to a reported study (14), $\langle\tau_{off}\rangle^{-1}$ and $\langle\tau_{on}\rangle^{-1}$ are the time-averaged product formation rate and dissociation rate of a single particle, respectively ($\langle\rangle$ denotes averaging) (26, 27). Therefore, the fluorescence turnover trajectories, such as the one shown in Fig. 2*B*, would allow us to study the catalytic kinetics and dynamics of an individual Au cluster. It should be noted that, under the laser intensity and the flow rate of solution used in the present study (14, 28), photobleaching or blinking of the fluorescent product resorufin is insignificant, compared with its short residence time on a particle. A continuous observation of such digital signals from individual clusters in a long-time window (>5 h) indicates a strong binding of individual clusters on slide. Further control experiments indicate that the strong binding or interaction between the slide and clusters only leads to negligible effect on the catalytic activity of clusters (*SI Appendix*).

To study the size-dependent catalysis of an individual Au cluster, by simply fixing the concentration of reductant NH$_2$OH (denoted as **A**), we obtained the average product formation rates and dissociation rates at different resazurin (denoted as **B**) concentrations. Interestingly, as shown in Fig. 3*A*, the product formation rates on both Au$_{18}$ and Au$_{25}$ clusters show saturated behavior with the concentration increase of resazurin, indicating a noncompetitive Langmuir–Hinshelwood mechanism (Fig. 3*B*, *Top*). This mechanism is described quantitatively by the following equations (6, 14, 29, 30):
Product formation rate:

$$\langle\tau_{off}\rangle^{-1} = \frac{\gamma_{eff}\alpha_B[S_B]}{1+\alpha_B[S_B]},\qquad [1]$$

and the product dissociation rate:

$$\langle\tau_{on}\rangle^{-1} = \frac{k_2 G_1[S_B]+k_3}{1+G_1[S_B]},\qquad [2]$$

where $[S_B]$ is the resazurin concentration; γ_{eff} is the rate constant representing the intrinsic reactivity per cluster for the catalytic conversion reaction; α_B is the adsorption equilibrium constant of resazurin; k_2 and k_3 are the rate constants for the indirect and direct dissociation of the product, respectively; $G_1 = k_1/(k_{-1}+k_2)$.

With the size decrease of Au clusters, unexpectedly, the product formation rate on Au clusters with only 15 Au atoms (Au$_{15}$) first increases with the substrate concentration (Fig. 3*C*), and then decreases after a maximum point. Similar behavior was also observed from the dependence of product formation rate on the reductant (NH$_2$OH) concentration as shown in *SI Appendix*, Fig. S5. As the decrease of product formation rate at high reactant

Fig. 1. Characterization of Au clusters. (*A*) UV-Vis absorption spectra and ESI-MS spectra (black lines in *Insets*) of the as-synthesized Au$_{15}$ (*Left*), Au$_{18}$ (*Middle*), and Au$_{25}$ (*Right*) clusters; the red arrows indicate characteristic absorption peaks of the corresponding Au nanoclusters. The red lines in the *Insets* are the simulated isotope patterns of [Au$_{15}$(MPA)$_{13}$ − 5 H + Na]$^{4-}$, [Au$_{18}$(MPA)$_{14}$ − 9 H + 5 Na]$^{4-}$, and [Au$_{25}$(MPA)$_{18}$ − 7 H + Na]$^{5-}$. (*B*) Typical TEM image of Au$_{25}$ clusters. (*Inset*) Typical high-angle annular dark-field imaging–TEM image of one Au$_{25}$ cluster. (*C*) Fluorescence spectra of resazurin reduction by NH$_2$OH catalyzed by Au$_{25}$ clusters (λ_{ex} = 532 nm; [resazurin] = 10 μM; [NH$_2$OH] = 20 mM). The arrow indicates fluorescence increase of the product with time.
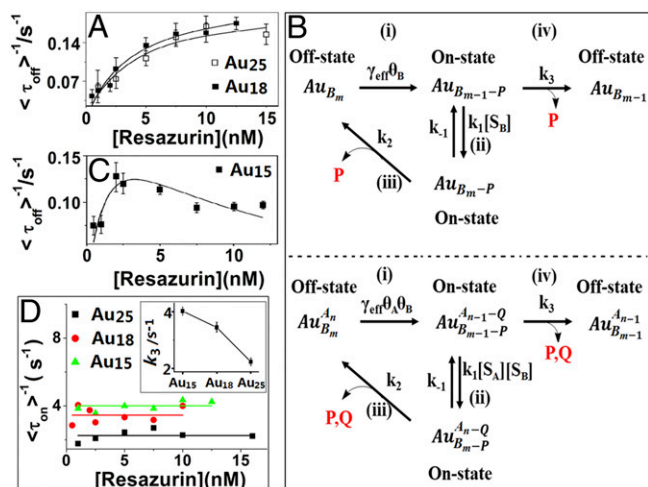
Fig. 3. Kinetic study of different-sized Au clusters. (*A* and *C*) Resazurin concentration titrations of $\langle\tau_{off}\rangle^{-1}$ on Au$_{25}$ (*A*), Au$_{18}$ (*A*), and Au$_{15}$ (*C*) with 20 mM NH$_2$OH. Each data point is averaged over the turnover trajectories of >50 clusters, with SEM as the error bar. The solid lines are fittings with Eqs. **1** (*A*) and **3** (*C*), respectively, with parameters summarized in *SI Appendix,* Table S1. (*B*, *Top*) Noncompetitive Langmuir–Hinshelwood mechanism of catalysis on a single nanoparticle. (*B*, *Bottom*) Competitive Langmuir–Hinshelwood mechanism of catalysis on a single nanoparticle. [A], the substrate NH$_2$OH concentration; [B], the substrate resazurin concentration; Au, Au nanoparticle; P, the product resorufin; Q, the product from NH$_2$OH. γ_{eff} represents the combined reactivity of all surface catalytic sites of a nanoparticle. k_1, k_{-1}, k_2, and k_3 are the rate constants at each steps. θ is the fraction of catalytic sites that are occupied by substrates. (*D*) Resazurin concentration dependence of $\langle\tau_{on}\rangle^{-1}$ of Au$_{15}$, Au$_{18}$, and Au$_{25}$. The solid lines are the fittings with constants. *Inset* is the size dependence of k_3.

concentration is not due to the gradual deactivation of Au clusters during the catalysis (*SI Appendix,* Fig. S6), all of these results suggest unambiguously a two-site competitive Langmuir–Hinshelwood mechanism (Fig. 3*B*, *Bottom*) between the two reactants, as described quantitatively by the following equations (29, 30):
Product formation rate:

$$\langle\tau_{off}\rangle^{-1} = \frac{\gamma_{eff}\alpha_A\alpha_B[S_A][S_B]}{(1 + \alpha_A[S_A] + \alpha_B[S_B])^2}, \qquad [3]$$

and the product dissociation rate:

$$\langle\tau_{on}\rangle^{-1} = \frac{k_2G[S_B] + k_3}{1 + G[S_B]}, \qquad [4]$$

where [S_A] is the NH$_2$OH concentration; α_A and α_B is the adsorption equilibrium constant of NH$_2$OH and resazurin, respectively; $G = [S_A]k_1/(k_{-1} + k_2)$.

However, the obtained dissociation rate on clusters is independent of the substrate concentration (Fig. 3*D*), which is different from the observed substrate concentration-dependent product dissociation behavior on traditional Au nanoparticles (6). Such independence of substrate concentration observed here on Au clusters could be for the following two reasons (14): (*i*) $k_2 = k_3$; and (*ii*) $k_1 = 0$. Due to the limited surface atoms or active sites on individual Au cluster for the substrate and/or product adsorption, after the adsorption of substrate molecules on the surface of an individual Au cluster reaches an equilibrium state, the binding of more substrate molecules would be hindered because of the steric hindrance effect without the release of substrate or product molecules, which means $k_1 = 0$ or the product molecules formed on the Au cluster surface could only be dissociated directly without the effect of substrate

molecules. Taken together, the right side of Eqs. **2** and **4** can be simplified as k_3, which is the rate constant of direct dissociation of the product.

By fitting the experimental data of the product formation rates and dissociation rates using the above equations and $k_1 = 0$ (Fig. 3 *A*, *C*, and *D*), the corresponding kinetic parameters for the product formation process (γ_{eff}, α_A, and α_B) and dissociation process (k_3) on different-sized Au clusters were obtained, and these data are included in *SI Appendix,* Table S1. Interestingly, these parameters clearly suggest a strong size-dependent relationship. In particular, γ_{eff} increases with the size decrease of Au clusters, which is consistent with an ensemble-level observation on the reported polyvinyl pyrrolidone-stabilized Au clusters (31); however, this result is contrary to a previous observation on individual Au nanoparticle (6). In addition, both the adsorption equilibrium constant (α_B) of the dye molecules and the direct product dissociation rate constant (k_3; Fig. 3*D*, *Inset*) decrease with the size increase of Au clusters, which is also contrary to a previous observation on Au nanoparticles (6). The decrease trend with the size increase indicates a strong adsorption of reactant resazurin and a weak adsorption of product resorufin molecules on small Au clusters.

To provide more insights on the size-dependent catalytic activity of Au clusters, the diameters (d in nanometers) of ligand-protected Au clusters (with size smaller than 2 nm) were calculated according to a reported equation: $n = 59$ atoms/nm$^3 \times 4/3 \times \pi \times (d/2)^3$ nm^3 (32), where N is the number of metal atoms per cluster (*SI Appendix*). As shown in *SI Appendix,* Table S1, the effective product formation rate constant per cluster (γ_{eff}) increases with the size decrease of Au clusters, which is contrary to the observation from Au nanoparticles (6). In addition, the intrinsic catalytic activity per surface area or active site [γ_{eff}/S, $S = 4\pi \times (d/2)^2$, the surface area of a single cluster; *SI Appendix,* Table S1] also increases with the size decrease of Au clusters, which agrees well with the observation from Au nanoparticles (6). For the Au clusters used in this study, the higher catalytic reactivity of smaller clusters is accompanied with a stronger substrate adsorption to (larger α_B) and a faster product desorption from (larger k_3) the catalytic sites of Au clusters (33). However, the apparently different size dependence of γ_{eff} between Au clusters and nanoparticles is probably for the following reason: $\gamma_{eff} \propto n_T \cdot (\gamma_{eff}/S)$, where n_T is the total number of active sites on a Au cluster or nanoparticle surface. For a nanoparticle with large number of surface atoms, the 2- to 3-nm decrease of size only leads to a small increase of γ_{eff}/S but results in a significant decrease of the number of surface active sites (n_T); therefore, the result is the decrease of γ_{eff} or $n_T \cdot (\gamma_{eff}/S)$ with the size decrease of nanoparticles. While for the Au clusters with size <2 nm (*SI Appendix,* Table S1), the value of γ_{eff}/S is very sensitive to the size (d) of clusters. For example, with a tiny decrease of size, such as from Au$_{18}$ to Au$_{15}$, the value of γ_{eff}/S remarkably increases, while the value of n_T only decreases slightly, therefore leading to the increase of γ_{eff} or $n_T \cdot (\gamma_{eff}/S)$ with the size decrease of clusters.

The above results show that the catalytic properties of clusters vary with size apparently. Further control experiments based on another type of Au clusters [Au$_{25}$(MHA)$_{18}$; MHA, 6-mercaptohexanoic acid; *SI Appendix,* Fig. S7 and Table S1] indicate that the observed difference of catalytic properties among clusters is not due to the ligand effect, instead, according to previous work (18, 19), such a difference could be attributed to the unique size or quantum electronic effect on the catalysis of Au clusters. However, the observed difference between small Au clusters and large nanoparticles could be attributed in part to their structural difference due to the fact that the atomic arrangements of small Au clusters are different from those of large nanoparticles.

Density Functional Theory Calculation for Cluster Size-Dependent Adsorption of Substrate and Product. Furthermore, to figure out why Au clusters with different sizes could catalyze the product formation process in different pathways, or why the reductant

NH$_2$OH could affect the adsorption of resazurin on the surface sites of small clusters, we carried out density functional theory (DFT) (*SI Appendix*) calculation to understand the adsorption of reactants and products on different-sized Au clusters. The data summarized in *SI Appendix*, Table S2 (first column), suggest that the intrinsic binding affinity of reactant resazurin is stronger on smaller-sized Au clusters. Such predicted size-dependent absorption of the reactant resazurin on Au clusters is consistent with the size-dependent adsorption equilibrium constant of the reactant (α_B) obtained experimentally from the single-molecule nanocatalysis, as shown in *SI Appendix*, Table S1. To further understand why the product formation on relatively larger clusters of Au$_{18}$ and Au$_{25}$ follows a noncompetitive Langmuir–Hinshelwood mechanism (Fig. 3*A*), while the catalysis of product formation on small Au$_{15}$ clusters follows a competitive Langmuir–Hinshelwood mechanism, we studied the effect of reductant NH$_2$OH on the adsorption of reactant resazurin (*SI Appendix*). Surprisingly, the results (*SI Appendix*, Table S2) indicate that the presence of NH$_2$OH can weaken the adsorption of resazurin on small Au$_{15}$ clusters, confirming the observed competitive mechanism on Au$_{15}$ cluster (Fig. 3*C*). In contrast, NH$_2$OH shows negligible effect on the adsorption of resazurin on Au$_{18}$ and Au$_{25}$ clusters, confirming the observed noncompetitive mechanism (Fig. 3*A*). The distinct difference of the catalytic mechanism between Au$_{15}$ and Au$_{18}$ clusters is probably due to the huge difference between their surface structures. As for the adsorption energy of product resorufin on Au clusters with different numbers of NH$_2$OH molecules around, interestingly, as shown in *SI Appendix*, Table S2, the adsorption energy of product decreases with the size decrease of Au clusters, which is consistent with the size-dependent k_3 shown in *SI Appendix*, Table S1. Such consistence indicates that the direct dissociation step of product resorufin can be affected by the reductant rather than the substrate resazurin, probably due to the unique surface structure of Au clusters.

Quantum Size Effect on Catalysis of Individual Clusters. According to a previous study (34), the specific catalytic activity of Au clusters could be attributed to the well-known quantum size effect. Wood derived an expression for the variation of metal work function as a function of the size (d in nanometers) of metal (35, 36):

$$W_d = W_\infty + \frac{1.08}{d}\,\text{eV},\qquad\qquad [5a]$$

where W_∞ is the bulk metal work function (5.10 eV for Au). Based on this, the variation in Fermi level energy (ε_f) of metals with the size of metal particles could be expressed as follows (35, 36):

$$\varepsilon_f = -\left(5.10\ \text{eV} + \frac{1.08}{d(\text{nm})}\,\text{eV}\right).\qquad [5b]$$

The energy spacing or gap (δ) between adjacent levels or electronic states could then be expressed by the following equation (37):

$$\delta = \varepsilon_f/N,\qquad\qquad\qquad [6a]$$

where N [$=59$ atoms/nm$^3 \times 4/3 \times \pi \times (d/2)^3$ nm] is the number of metal atoms per ligand-protected Au cluster (with size smaller than 2 nm) (32). Substituting ε_f in Eq. **6a** with Eq. **5b** and considering δ as positive, the relationship between δ and d can be expressed as follows:

$$\delta = \left(0.16/d^3 + 0.0352/d^4\right)\text{eV}.\qquad [6b]$$

Accordingly, the δ values of Au clusters with different sizes were obtained, as shown in *SI Appendix*, Table S1. It shows that the energy gap of Au clusters decreases with the size increase of Au clusters.

Recently, Häkkinen and coworkers (38) observed a positive linear correlation between the energy gap (δ) and the adsorption energy or binding ability of O$_2$ on Au clusters. Based on it, we hold the opinion that the adsorption equilibrium constant (α) of reactants on Au clusters could probably be expressed as follows:

$$\alpha = K_1 \cdot \delta = K_1\left(0.16/d^3 + 0.0352/d^4\right).\qquad [7]$$

K_1 is the proportional factor between α and δ. It indicates that the adsorption or binding ability of O$_2$ on clusters decreases with the increasing of the cluster size (d), which is consistent with the experimental observation of resazurin adsorption (α_B; *SI Appendix*, Table S1) on Au clusters, but contrary to the observed resazurin adsorption on Au nanoparticles (*SI Appendix*, Table S1) (6). Such differences between Au clusters and nanoparticles could be mainly attributed to the unique size effect on catalysis of clusters (38). As for the resazurin adsorption (α_B) on Au clusters (*SI Appendix*, Table S1), by fitting the d-dependent α_B with Eq. 7 (Fig. 4*A*), the value of K_1 was obtained to be 1,530 ± 318 μM^{-1}·eV^{-1}.

However, it was further found that the correlation shown in Eq. 7 does work for some adsorbates (such as O$_2$ and resazurin) but not for all on Au clusters. Actually, it has been reported that the CO adsorption ability increases monotonically with Au cluster size due to the more favorable LUMO (M)–σ(CO) interaction for larger clusters (39). Interestingly, such CO adsorption on Au clusters is consistent with the observed adsorption of product resorufin on Au clusters indicated by the dissociation rate (large k_3) of resorufin from Au clusters (*SI Appendix*, Table S1). While the difference of adsorption properties observed between substrate resazurin and product resorufin on the same set of Au clusters probably could be attributed to the different electronic interactions between clusters and these two types of molecules, while such different electronic interactions could be further attributed to the structural/compositional differences between substrate resazurin and product resorufin.

Moreover, as *SI Appendix*, Table S1 shows, the catalytic activity and the adsorptions of both substrate and product molecules correlate with the work function (W_d) (obtained from Eq. **5a**) of clusters in the same manners as that with the energy gap (δ) due to the similar size (d) dependences of W_d (Eq. **5a**) and δ (Eq. **6b**).

Moreover, for the Au clusters used in this study, unexpectedly, Fig. 4*B* shows a linear correlation between the catalytic reactivity (γ_{eff}/S, the catalytic rate constant per surface area) and substrates binding (α_B) to the Au clusters, with a slope of $K_2 = 0.32 \pm 0.01$ s^{-1}·nm^{-2}·μM, the proportional factor between α and γ_{eff}/S.
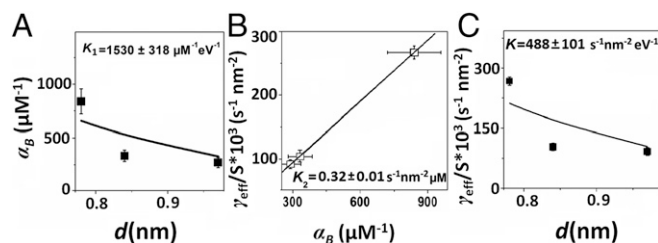

Fig. 4. Size-dependent catalytic kinetics of Au clusters. (*A*) Size dependence of the adsorption equilibrium constant of resazurin (α_B), where the solid line is the fittings according to Eq. 7. (*B*) The correlation analysis between the effective rate constant per surface area (γ_{eff}/S) and the adsorption equilibrium constant of resazurin (α_B), where the solid line is the linear fitting. (*C*) Size dependence of the effective rate constant per surface area (γ_{eff}/S), where the solid line is the fitting according to Eq. 8.

Thus, the relationship between γ_{eff}/S and δ or d can be expressed as follows:

$$\gamma_{\text{eff}}\bigg/S = K_2 \cdot \alpha = K_2 \cdot K_1 \cdot \delta = K\left(\frac{0.16}{d^3} + \frac{0.0352}{d^4}\right), \quad \text{[8]}$$

where $K = K_2 \cdot K_1$. By fitting the d-dependent γ_{eff}/S with Eq. **8** (Fig. 4C), we obtained the proportionality constant K (488.3 ± 101.4 s^{-1}·nm^{-2}·eV^{-1}), and then $K_2 = K/K_1 = 0.32$ s^{-1}·nm^{-2}·μM, which is exactly the same as that obtained from Fig. 4B ($K_2 = 0.32 \pm 0.01$ s^{-1}·nm^{-2}·μM). These data confirm the reliability of the linear relationship between the energy gap and adsorption energy (38), and the linear relationship between the catalytic rate constant and binding ability of substrate to Au clusters (Fig. 4B). Both of these two linear relationships observed on Au clusters are due to the unique size effect on the catalysis of Au clusters (37).

As for the higher catalytic activity of smaller Au clusters (shown in *SI Appendix*, Table S1), besides the contribution from the quantum size effect as discussed above, a ligand effect was also observed. The Au 4f$_{7/2}$ XPS spectra (*SI Appendix*, Fig. S8A) on different clusters show clear positive shift of binding energy with the size decrease. Due to the positive correlation between the binding energies and sulfur (S) contents (Au$_{25}$ with S 41 wt%, Au$_{18}$ with S 43 wt%, and Au$_{15}$ with S 46 wt%) on different clusters (*SI Appendix*, Fig. S8B), the positive shift of binding energy with the size decrease could be attributed to the stronger interaction between Au and sulfur in the form of Au–S bonding. It has been known that the higher binding energy of metal nanocatalysts usually corresponds to higher catalytic activity (40); therefore, the higher catalytic activity of smaller Au clusters observed in this study could be partially attributed to the ligands effect (41, 42).

Size-Dependent Catalytic Dynamics of Individual Clusters. Similar to previous nanoparticle studies (6, 14), to study the catalytic dynamics of individual Au clusters, we further determined the activity fluctuations of individual Au clusters. The activity fluctuations could be reflected by the reaction rate variations in the τ_{off} reaction (the catalytic product formation), the τ_{on} reaction (the product dissociation), or both. To study the activity fluctuations of τ_{off} and τ_{on} processes, we extracted the sequences of individual τ_{off} and τ_{on} from each turnover trajectory, and then calculated their autocorrelation functions, $C_\tau(m) = \langle \Delta\tau(0)\Delta\tau(m)\rangle/\langle\Delta\tau^2\rangle$ (43, 44). Here, τ is either τ_{off} or τ_{on}, m is the turnover index number in the sequence, and $\Delta\tau(m) = \tau(m) - \langle\tau\rangle$. With activity fluctuations, the values of $C\tau(m)$ are positive and show a decay behavior with the decay time constant being the fluctuation correlation time. Fig. 5 A and B show exemplary $C\tau_{\text{off}}(m)$ and $C\tau_{\text{on}}(m)$ of a single Au$_{15}$ cluster. The exponential decay behaviors of $C\tau_{\text{off}}(m)$ and $C\tau_{\text{on}}(m)$ directly demonstrate the activity fluctuations in the catalytic product formation and dissociation reaction, respectively. For the single cluster shown in Fig. 5 A and B, the exponential decay constant of $C\tau_{\text{off}}(m)$ is $m_{\text{off}} = 5.0 \pm 0.4$ turnovers, and that of $C\tau_{\text{on}}(m)$ is $m_{\text{on}} = 1.2 \pm 0.2$ turnovers. With an average turnover time of ~11.2 s for this particular cluster, the activity fluctuation correlation time for its τ_{off} and τ_{on} reactions is ~56 and ~13 s, respectively. These two correlation times are the timescales of the catalysis-induced dynamic conformation restructuring of the clusters (45, 46). The activity fluctuation of individual clusters could be attributed to small-scale dynamic conformation restructuring, similar to that of nanoparticles (6, 14). While for Au clusters with small number of atoms here, changing adsorbate–surface interactions during catalysis can induce a dynamic conformation reconstruction, resulting in oscillatory kinetics due to the different activities of different surface structures. Moreover, compared with the distribution of fluctuation correlation time of Au nanoparticles (the width of the time distribution is about 400 s) (6, 14), the distributions (Fig. 5 A and B, Insets) of the fluctuation correlation time of Au clusters are much narrower (the width of the time distribution is about 170 s), indicating that individual clusters have more
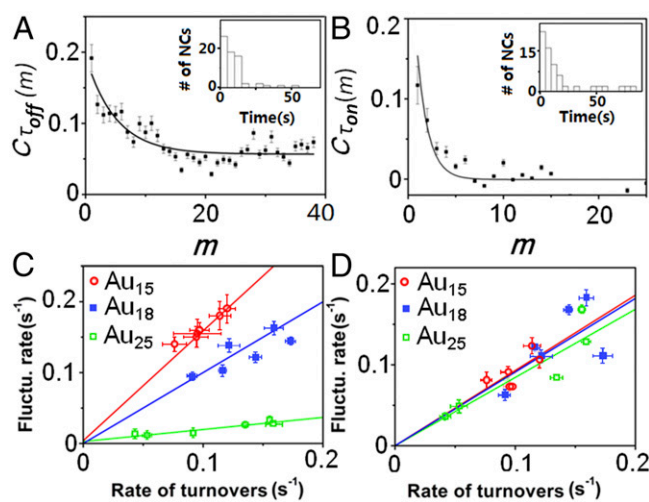

Fig. 5. (A and B) Autocorrelation function of the τ_{off} (A) and τ_{on} (B) from the turnover trajectory of a single Au$_{15}$ cluster at 10 nM resazurin. The solid lines are the exponential fits with decay constants of $m_{\text{off}} = 5.0 \pm 0.4$ turnovers and $m_{\text{on}} = 1.2 \pm 0.2$ turnovers. (*Inset*) Histograms of the fluctuation correlation times for τ_{off} and τ_{on} reactions at 10 nM resazurin. (C and D) Dependence of the activity fluctuation rate (the inverse of fluctuation correlation time) of the τ_{off} reaction (C) and the τ_{on} reaction (D) on the rate of turnovers. Each data point is an average from >50 trajectories. Error bars are SEM. The solid lines are linear fits.

consistent restructuring timescales, probably due to their much narrower size distribution compared with Au nanoparticles.

Furthermore, the catalysis-induced activity fluctuations or surface restructuring were also observed from the positive correlations between the activity fluctuation rates (i.e., the inverse of fluctuation correlation times) and the turnover rates (Fig. 5 C and D). It shows that the activity fluctuation rates of both τ_{off} and τ_{on} reactions increase with the increase of turnover rates, following a linear correlation approximately. Interestingly, the slope of such linear correlation increases with the size decrease of Au clusters for both τ_{off} and τ_{on} reactions. Such size dependence indicates that the catalysis of smaller Au clusters can induce a faster dynamic surface restructuring, which is consistent with the observation on Au nanoparticles (6). Moreover, Fig. 5 C and D further suggest that the slope of the τ_{off} reaction (Fig. 5C) increases faster with the size decrease than that of the τ_{on} reaction (Fig. 5D), indicating that τ_{off} reaction-induced activity fluctuations or surface restructuring is more sensitive to the size of Au clusters than τ_{on} reaction-induced activity fluctuations or surface restructuring, which is contrary to the observation on Au nanoparticles (6). Furthermore, as shown in Fig. 5 C and D, the activity fluctuation rates were extrapolated linearly to zero rate of turnovers for all three Au clusters. The positive intercepts approximate the rates of spontaneous (compared with the catalysis-induced restructuring) dynamic surface restructuring of individual Au clusters in an aqueous environment, but the small values (approximately zero) of these intercepts indicate that the spontaneous dynamic surface restructuring of Au clusters could be neglected, compared with the catalysis-induced restructuring (Fig. 5 C and D). Such observation indicates that the surface of Au clusters is more stable than the surface of Au nanoparticles in aqueous environment since the remarkable spontaneous surface restructuring has been observed on Au nanoparticles (6). Such differences observed above between Au clusters and nanoparticles could be partially attributed to the strong stabilization of MPA ligands to the surface Au atoms.

It should be noted that the size-dependent catalytic properties of Au clusters revealed here intrinsically could be attributed to their size-dependent structures, such as size-sensitive electronic structure (charge density profile). The tiny fluctuation of the

electronic structure induced by the size variation of clusters can hugely affect the interaction between the clusters and the substrate or product molecules.

Conclusions

The size-dependent catalytic activity of Au clusters under ambient solution conditions was studied at the single-molecule, single-cluster level. Atomically precise Au clusters with different sizes show distinct catalytic kinetics and mechanisms with different substrate and product adsorption ability. In particular, the smaller Au_{15} cluster follows a competitive Langmuir–Hinshelwood mechanism with stronger substrate binding ability and weaker product binding ability, while the larger ones, Au_{18} and Au_{25} clusters, follow a noncompetitive Langmuir–Hinshelwood mechanism with weaker substrate binding ability and stronger product binding ability. DFT calculation suggests that such size-dependent catalytic activities and catalytic mechanisms could be attributed to the different adsorption behaviors of substrate and product molecules on clusters with different sizes, which are intrinsically induced by the size-dependent electronic structures of the Au clusters. The analysis of dynamic activity fluctuations and surface reconstruction of the Au clusters revealed more different catalytic properties between Au clusters and traditional Au nanoparticles due to the unique size-dependent properties of clusters. The knowledge obtained here at the single-cluster level provides fundamental insights into the catalytic behaviors of cluster catalysts, which are complementary to, and often inaccessible in ensemble-averaged measurements.

Experimental Procedures

The MPA-protected Au clusters were synthesized according to a reported protocol (25). All single-molecule nanocatalysis was carried out in home-built flow cells, which were formed by double-sided tapes sandwiched between a quartz slide (Technical Glass) and a coverslip (Gold Seal). The solution was flowed into the cell with a flow rate of 10 μL·min^{-1}. A continuous-wave circularly polarized 532-nm laser was focused onto an area of about 90×50 μm^2 on the sample to directly excite the fluorescence of the product resorufin. The fluorescence of resorufin was collected by a water-immersion objective, filtered by two filters and projected onto an EMCCD camera (Andor Technology), which is controlled by Andor IQ software.

1. Haruta M, Kobayashi T, Sano H, Yamada N (1987) Novel gold catalysts for the oxidation of carbon-monoxide at a temperature far below 0 °C. *Chem Lett* 2:405–408.
2. Haruta M, Yamada N, Kobayashi T, Iijima S (1989) Gold catalysts prepared by coprecipitation for low-temperature oxidation of hydrogen and of carbon-monoxide. *J Catal* 115:301–309.
3. Somorjai GA (2000) The development of molecular surface science and the surface science of catalysis: The Berkeley contribution. *J Phys Chem B* 104:2969–2979.
4. Bergeret G, Gallezot P, Ertl G, Knözinger H, Weitkamp J (1997) *Handbook of Heterogeneous Catalysis* (VCH, Weinheim, Germany).
5. Tong X, et al. (2005) Intact size-selected Au(n) clusters on a TiO2(110)-(1 × 1) surface at room temperature. *J Am Chem Soc* 127:13516–13518.
6. Zhou X, Xu W, Liu G, Panda D, Chen P (2010) Size-dependent catalytic activity and dynamics of gold nanoparticles at the single-molecule level. *J Am Chem Soc* 132:138–146.
7. Fenger R, Fertitta E, Kirmse H, Thünemann AF, Rademann K (2012) Size dependent catalysis with CTAB-stabilized gold nanoparticles. *Phys Chem Chem Phys* 14:9343–9349.
8. Chen P, et al. (2014) Spatiotemporal catalytic dynamics within single nanocatalysts revealed by single-molecule microscopy. *Chem Soc Rev* 43:1107–1117.
9. Chen P, et al. (2010) Single-molecule fluorescence imaging of nanocatalytic processes. *Chem Soc Rev* 39:4560–4570.
10. Orrit M, Ha T, Sandoghdar V (2014) Single-molecule optical spectroscopy. *Chem Soc Rev* 43:973–976.
11. Janssen KPF, et al. (2014) Single molecule methods for the study of catalysis: From enzymes to heterogeneous catalysts. *Chem Soc Rev* 43:990–1006.
12. De Cremer G, Sels BF, De Vos DE, Hofkens J, Roeffaers MBJ (2010) Fluorescence micro(spectro)scopy as a tool to study catalytic materials in action. *Chem Soc Rev* 39:4703–4717.
13. Chen T, Zhang Y, Xu W (2016) Size-dependent catalytic kinetics and dynamics of Pd nanocubes: A single-particle study. *Phys Chem Chem Phys* 18:22494–22502.
14. Xu W, Kong JS, Yeh Y-TE, Chen P (2008) Single-molecule nanocatalysis reveals heterogeneous reaction pathways and catalytic dynamics. *Nat Mater* 7:992–996.
15. Chen P, Xu W, Zhou X, Panda D, Kalininskiy A (2009) Single-nanoparticle catalysis at single-turnover resolution. *Chem Phys Lett* 470:151–157.
16. Tachikawa T, Yamashita S, Majima T (2011) Evidence for crystal-face-dependent TiO2 photocatalysis from single-molecule imaging and kinetic analysis. *J Am Chem Soc* 133:7197–7204.
17. Wang N, Tachikawa T, Majima T (2011) Single-molecule, single-particle observation of size-dependent photocatalytic activity in Au/TiO2 nanocomposites. *Chem Sci* 2:891–900.
18. Tyo EC, Vajda S (2015) Catalysis by clusters with precise numbers of atoms. *Nat Nanotechnol* 10:577–588.
19. Kappes MM, Radi P, Schar M, Schumacher E (1985) Probes for electronic and geometrical shell structure effects in alkali-metal clusters. Photoionization measurements on KₓLi, KₓMg and KₓZn (x < 25). *Chem Phys Lett* 119:11–16.
20. Kappes MM, Kunz RW, Schumacher E (1982) Production of large sodium clusters (Naₓ, x < 65) by seeded beam expansions. *Chem Phys Lett* 91:413–418.
21. Bergeron DE, Castleman AW, Jr, Morisato T, Khanna SN (2004) formation of Al₁₃I⁻: Evidence for the superhalogen character of Al13. *Science* 304:84–87.
22. Böhme DK, Schwarz H (2005) Gas-phase catalysis by atomic and cluster metal ions: The ultimate single-site catalysts. *Angew Chem Int Ed Engl* 44:2336–2354.
23. Yu Y, et al. (2014) Identification of a highly luminescent Au22(SG)18 nanocluster. *J Am Chem Soc* 136:1246–1249.
24. Ye R, Zhukhovitskiy AV, Deraedt CV, Toste FD, Somorjai GA (2017) Supported dendrimer-encapsulated metal clusters: Toward heterogenizing homogeneous catalysts. *Acc Chem Res* 50:1894–1901.
25. Yu Y, et al. (2013) Scalable and precise synthesis of thiolated Au10-12, Au15, Au18, and Au25 nanoclusters via pH controlled CO reduction. *Chem Mater* 25:946–952.
26. Xu WL, Kong JS, Chen P (2009) Single-molecule kinetic theory of heterogeneous and enzyme catalysis. *J Phys Chem C* 113:2393–2404.
27. Xu WL, Shen H, Liu GK, Chen P (2009) Single-molecule kinetics of nanoparticle catalysis. *Nano Res* 2:911–922.
28. Chen T, Zhang Y, Xu W (2016) Single-molecule nanocatalysis reveals catalytic activation energy of single nanocatalysts. *J Am Chem Soc* 138:12414–12421.
29. Satterfield CN (1980) *Heterogeneous Catalysis in Practice* (McGraw-Hill, New York).
30. Han KS, Liu G, Zhou X, Medina RE, Chen P (2012) How does a single Pt nanocatalyst behave in two different reactions? A single-molecule study. *Nano Lett* 12:1253–1259.
31. Tsunoyama H, et al. (2011) Size-controlled synthesis of gold clusters as efficient catalysts for aerobic oxidation. *Catal Surv Asia* 15:230–239.
32. Jin R (2010) Quantum sized, thiolate-protected gold nanoclusters. *Nanoscale* 2:343–362.
33. Strizhak PE (2013) Nanosize effects in heterogeneous catalysis. *Theor Exp Chem* 49:2–21.
34. Valden M, Lai X, Goodman DW (1998) Onset of catalytic activity of gold clusters on titania with the appearance of nonmetallic properties. *Science* 281:1647–1650.
35. Wood DM (1981) Classical size dependence of the work function of small metallic spheres. *Phys Rev Lett* 46:749.
36. Phala NS, Steen Ev (2007) Intrinsic reactivity of gold nanoparticles: Classical, semi-empirical and DFT studies. *Gold Bull* 40:150–153.
37. Kubo R (1962) Electronic properties of metallic fine particles. I. *J Phys Soc Jpn* 17:975–986.
38. Lopez-Acevedo O, Kacprzak KA, Akola J, Häkkinen H (2010) Quantum size effects in ambient CO oxidation catalysed by ligand-protected gold clusters. *Nat Chem* 2:329–334.
39. Lee TH, Ervin KMJ (1994) Reactions of copper group cluster anions with oxygen and carbon monoxide. *J Phys Chem* 98:10023–10031.
40. Ruan M, Sun X, Zhang Y, Xu W (2015) Regeneration and enhanced catalytic activity of Pt/C electrocatalysts. *ACS Catal* 5:233–240.
41. Tsunoyama H, Ichikuni N, Sakurai H, Tsukuda T (2009) Effect of electronic structures of Au clusters stabilized by poly(N-vinyl-2-pyrrolidone) on aerobic oxidation catalysis. *J Am Chem Soc* 131:7086–7093.
42. Chaki NK, Tsunoyama H, Negishi Y, Sakurai H, Tsukuda T (2007) Effect of Ag-doping on the catalytic activity of polymer-stabilized au clusters in aerobic oxidation of alcohol. *J Phys Chem C* 111:4885–4888.
43. Lu HP, Xun L, Xie XS (1998) Single-molecule enzymatic dynamics. *Science* 282:1877–1882.
44. Witkoskie JB, Cao J (2004) Single molecule kinetics. I. Theoretical analysis of indicators. *J Chem Phys* 121:6361–6372.
45. Imbihl R, Ertl G (1995) Oscillatory kinetics in heterogeneous catalysis. *Chem Rev* 95:697–733.
46. Newton MA, Belver-Coldeira C, Martínez-Arias A, Fernández-García M (2007) Dynamic in situ observation of rapid size and shape change of supported Pd nanoparticles during CO/NO cycling. *Nat Mater* 6:528–532.

CHEMISTRY